

RESEARCH ARTICLE

10.1002/2016JD025617

Key Points:

- CO₂ signals predicted for California tower and satellite observations
- Estimated inversion uncertainties in posterior fossil and biosphere exchanges
- Posterior uncertainties reduced for major urban and agricultural regions

Correspondence to:

M. L. Fischer,
mlfischer@lbl.gov

Citation:

Fischer, M. L., et al. (2017), Simulating estimation of California fossil fuel and biosphere carbon dioxide exchanges combining in situ tower and satellite column observations, *J. Geophys. Res. Atmos.*, 122, 3653–3671, doi:10.1002/2016JD025617.









Received 5 JUL 2016

Accepted 7 MAR 2017

Accepted article online 9 MAR 2017

Published online 25 MAR 2017

Simulating estimation of California fossil fuel and biosphere carbon dioxide exchanges combining in situ tower and satellite column observations

Marc L. Fischer¹ , Nicholas Parazoo² , Kieran Brophy³, Xinguang Cui¹ , Seongeun Jeong¹ , Junjie Liu⁴ , Ralph Keeling⁵, Thomas E. Taylor⁶, Kevin Gurney⁷ , Tomohiro Oda^{8,9} , and Heather Graven³ 

¹Lawrence Berkeley National Laboratory, Berkeley, California, USA, ²Jet Propulsion Laboratory, California Institute of Technology, Pasadena, California, USA, ³Department of Physics, Imperial College London, London, UK, ⁴Jet Propulsion Laboratory, Pasadena, California, USA, ⁵Scripps Institution of Oceanography, University of California, San Diego, La Jolla, California, USA, ⁶Cooperative Institute for Research in the Atmosphere, Colorado State University, Fort Collins, Colorado, USA, ⁷School of Life Sciences, Arizona State University, Tucson, Arizona, USA, ⁸Global Modeling and Assimilation Office, NASA Goddard Space Flight Center, Greenbelt, Maryland, USA, ⁹Goddard Earth Sciences Technology and Research, Universities Space Research Association, Columbia, Maryland, USA

Abstract We report simulation experiments estimating the uncertainties in California regional fossil fuel and biosphere CO₂ exchanges that might be obtained by using an atmospheric inverse modeling system driven by the combination of ground-based observations of radiocarbon and total CO₂, together with column-mean CO₂ observations from NASA's Orbiting Carbon Observatory (OCO-2). The work includes an initial examination of statistical uncertainties in prior models for CO₂ exchange, in radiocarbon-based fossil fuel CO₂ measurements, in OCO-2 measurements, and in a regional atmospheric transport modeling system. Using these nominal assumptions for measurement and model uncertainties, we find that flask measurements of radiocarbon and total CO₂ at 10 towers can be used to distinguish between different fossil fuel emission data products for major urban regions of California. We then show that the combination of flask and OCO-2 observations yields posterior uncertainties in monthly-mean fossil fuel emissions of ~5–10%, levels likely useful for policy relevant evaluation of bottom-up fossil fuel emission estimates. Similarly, we find that inversions yield uncertainties in monthly biosphere CO₂ exchange of ~6%–12%, depending on season, providing useful information on net carbon uptake in California's forests and agricultural lands. Finally, initial sensitivity analysis suggests that obtaining the above results requires control of systematic biases below approximately 0.5 ppm, placing requirements on accuracy of the atmospheric measurements, background subtraction, and atmospheric transport modeling.

1. Introduction

California is the most populous state in the U.S. and presently emits approximately 100 Tg C yr⁻¹ of CO₂ from fossil fuel use [California Air Resources Board (CARB), 2015], roughly 1% of the global total emissions [Boden et al., 2016]. In 2006, California's "Global Warming Solutions Act" (AB-32) set a goal of reducing greenhouse gas emissions 15% by 2020, compared to business-as-usual growth in emissions; further reductions of 40% are planned for 2030, and 80% by 2050. Estimates of fossil fuel CO₂ (ffCO₂) emissions commonly use "bottom-up" calculations that integrate activity data, such as fuel consumption, with emission factors that describe how much ffCO₂ is emitted per unit of activity. Bottom-up estimates of ffCO₂ emissions are reported to have small uncertainties of ±5% (1σ) at the global level [Le Quéré et al., 2015], but they can be subject to biases from missing sources or errors in emission factors, and uncertainties can become much larger on subnational scales [Asefi-Najafabady et al., 2014; Hogue et al., 2016].

Inversions of atmospheric data including fossil fuel tracers such as radiocarbon could provide independent estimates for regional emissions of fossil fuel-derived CO₂ in California. Fossil fuel-derived CO₂ can be distinguished with observations of radiocarbon (¹⁴C) in CO₂ because fossil fuels have lost all ¹⁴C to radioactive decay [Levin et al., 2003]. Other tracers of fossil fuel-derived CO₂ include carbon monoxide (CO), nitrogen oxides (e.g., NO₂) [Konovalov et al., 2016], or synthetic gases such as sulfur hexafluoride [Turnbull et al., 2006]. Atmospheric data have been used previously to provide independent short-term estimates for

emissions of ffCO_2 from different regions of California. For example, *Turnbull et al.* [2011] analyzed radiocarbon flask data collected as part of an aircraft mass balance study in February 2009 that found fossil fuel CO_2 emissions from Sacramento county were approximately consistent with the Vulcan bottom-up emission data product for 2002 [*Gurney et al.*, 2009] (mean difference relative to Vulcan: -17% , range: -43% to $+133\%$). As part of the California Research at the Nexus of Air Quality and Climate Change study in May–June 2010, an analysis of continuous in situ CO_2 and CO collected in Pasadena, California found that ffCO_2 was consistent ($-3\% \pm 14\%$) with signals computed by using the Vulcan model [*Newman et al.*, 2013], while a separate tracer-ratio inversion of aircraft total CO_2 and CO observations from six daytime flights estimated fossil fuel CO_2 emissions that were somewhat higher ($15\text{--}38\%$) than Vulcan [*Brioude et al.*, 2013].

Atmospheric data may also provide valuable constraints on state and regional carbon exchange by terrestrial ecosystems in California. Net biosphere fluxes are the result of differences between large gross uptake and respiration fluxes, each of which depends on a combination of vegetation cover, seasonally varying climate, and often to a large degree, land management. While California forests were recently estimated to sequester $\sim 13 \text{ Tg C yr}^{-1}$ [*CARB*, 2015], the net uptake is uncertain and may be highly variable from year to year. For example, California's ecosystems are estimated to switch to a net source in dry years [*Potter*, 2010]. In addition, agriculture in California may not be carbon neutral [*Wolf et al.*, 2015] and changes in agricultural practices have the potential to sequester carbon in agricultural systems.

Here we explore the potential for a prototype data collection and data analysis system to estimate regional and state-total fossil and biosphere CO_2 (bioCO_2) exchanges in California by using simulation experiments. The simulated atmospheric observations include remotely sensed column-averaged CO_2 dry air mole fraction (denoted as XCO_2) from NASA's Orbiting Carbon Observatory Satellite (OCO-2) [*Crisp et al.*, 2017] and tower-based observations of CO_2 concentrations, in conjunction with radiocarbon in CO_2 , which enables separation of fossil fuel and biospheric influences from CO_2 in flask samples. The use of both satellite and tower platforms combines the spatial coverage of OCO-2 with the additional tracer data provided by the ground-based network. Recently, *Basu et al.* [2016] performed a similar simulation experiment to determine regional and U.S. total ffCO_2 and bioCO_2 exchanges by using the CarbonTracker inversion system with radiocarbon samples from tower sites spread across the continental United States. They found that regional ffCO_2 emissions could generally be estimated to within $\pm 5\%$ with a high-density tower network and that regional uncertainty in estimated biosphere exchanges was reduced with the use of radiocarbon data. In comparison to *Basu et al.*, we focus on the smaller domain of California by using a mesoscale atmospheric transport model and include column CO_2 data. At urban scales, simulation experiments have also investigated the degree to which CO_2 emissions could be estimated for subsectors of fossil fuel use by using networks of tower-based CO_2 sensors [*Kort et al.*, 2013; *Wu et al.*, 2016].

In section 2 we describe an observing system simulation experiment that simulates ffCO_2 and bioCO_2 signals for a planned deployment of air samplers at 10 existing tower sites in combination with OCO-2 XCO_2 retrievals over California. We then describe a regionally specific inversion framework used to solve for expected posterior uncertainties in fossil fuel and biosphere exchanges for 2 months: November 2010 and May 2011. In the results we report the simulated fossil and biosphere CO_2 signals for the tower sites and OCO-2, the uncertainties in posterior ffCO_2 and bioCO_2 exchanges by region and in total by using (a) OCO-2 data alone, (b) flask data alone, or (c) the combination of OCO-2 and flasks together. We then conduct initial sensitivity analyses of three varieties. First we vary the assumptions for random uncertainties in prior emissions and the model-measurement comparison. Next, we explore biases introduced in posterior statewide fossil fuel CO_2 emissions when regional inversion scheme is supplied with spatially "incorrect" prior emission models (i.e., differing from the emission model used to calculate simulated observations). Last, we also explore the sensitivity of posterior estimates of statewide CO_2 exchange to examples of potential observational and transport model biases.

2. Methods

As described above, this work explores the application of flask measurements of CO_2 and radiocarbon in CO_2 and remote sensing of total CO_2 to quantify California's regional CO_2 exchanges at regional and statewide scales. The analysis approach applies a Bayesian inversion developed for previous work to estimate methane emissions that combine atmospheric observations, atmospheric transport modeling, prior flux models, and

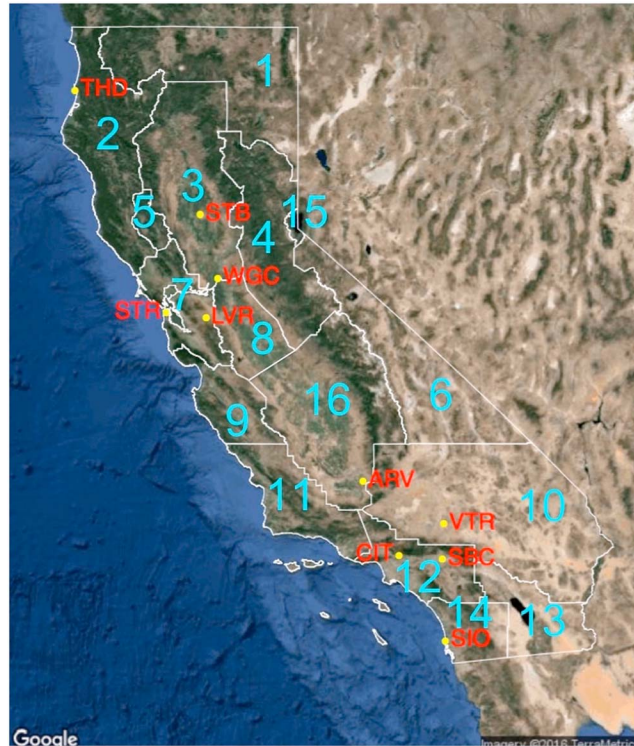


Figure 1. Map of California showing 10 tower sampling sites and 16 regions for which CO₂ exchanges are estimated.

2 days at 2200 UT (1400 PST) at each site over two example months when net biosphere exchange of CO₂ is expected to be positive (November 2010) and negative (May 2011). While we do not include continuous measurements of total CO₂ or combustion tracers (e.g., CO or NO₂) in this analysis, we note that the addition of continuous data has the potential to improve the estimates of CO₂ exchange and might reasonably be included in a future study.

The amount of CO₂ added by fossil fuel emissions (ffCO₂) and the amount of CO₂ added or removed by biospheric exchange (bioCO₂) can be calculated in flask air by using measurements of radiocarbon in CO₂ (Δ¹⁴C) as following the work of *Levin et al.* [2003]:

$$ffCO_2 = C_{obs} \frac{\Delta_{bg} - \Delta_{obs}}{\Delta_{bg} - \Delta_{ff}} + \beta, \tag{1}$$

$$bioCO_2 = C_{obs} - C_{bg} - ffCO_2. \tag{2}$$

Table 1. Tower Measurement Sites

Site	Location	Latitude	Longitude	Inlet Height (m, agl)
ARV	Arvin	35.24	-118.79	10
CIT	Caltech, Pasadena	34.14	-118.12	10
LVR	Livermore	37.67	-121.71	27
SBC	San Bernardino	34.09	-117.31	58
SIO	Scripps	32.87	-117.26	10
STB	Sutter Buttes	39.21	-121.82	10
STR	San Francisco	37.76	-122.45	232
THD	Trinidad Head	41.05	-124.15	20
VTR	Victorville	34.61	-117.29	90
WGC	Walnut Grove	38.27	-121.49	91

uncertainty specification [*Jeong et al.*, 2013]. As in the previous work, the inversion multiplicatively scales prior emission estimates in 16 regions (see Figure 1) that are slightly modified from the 15 “air basins” classified by the California Air Resources Board for air quality control (<https://www.arb.ca.gov/design/adm/basinconty.htm>), subdividing the San Joaquin Valley into northern (region 8) and southern (region 16) subregions.

2.1. Observation Network

2.1.1. Tower Network for ffCO₂ and BioCO₂

The prototype observation system we investigate here is based on a similar network used for a 2 month ground-based measurement campaign at 10 existing air sampling sites located in major urban and selected rural areas across California (Figure 1 and Table 1). Here we assumed that flask samples would be collected every

Here C_{obs} and Δ_{obs} are the observed atmospheric CO₂ mixing ratio and the Δ¹⁴C ratio of the observed CO₂, C_{bg} and Δ_{bg} are the background CO₂ concentration and isotopic ratio, Δ_{ff} is the isotopic ratio of pure fossil fuel combustion (−1000‰), and β represents the effect of nonfossil isotopic influences on the calculation of ffCO₂. The equations derive from approximate mass balances for ¹⁴CO₂ and total CO₂ and are expressed in

units of ppm. C_{bg} and Δ_{bg} represent the composition of air entering California, which can be determined by observations at coastal sites under conditions with persistent marine air inflow [Li *et al.*, 2005]. In this study, we do not explicitly employ estimates of C_{bg} or Δ_{bg} but do include an estimate of how uncertainties in these parameters propagate into uncertainty in local signals as described below.

Uncertainty in measuring $ffCO_2$ and $bioCO_2$ is composed of contributions from each of the terms in equation (1) but typically dominated by measurement uncertainties in Δ_{obs} and Δ_{bg} . Here uncertainty in each measurement of $\Delta^{14}C$ is roughly 2‰ [Graven *et al.*, 2007], equivalent to ~ 0.8 ppm in $ffCO_2$. By comparison, measurement uncertainty in the total CO_2 concentration is typically near 0.1 ppm [Keeling *et al.*, 2001], negligible in comparison to uncertainty in $\Delta^{14}C$. Previous observations have shown that $\Delta^{14}C$ gradients in background air in the Northern Hemisphere between La Jolla, California (latitude $\sim 26^\circ N$) and Point Barrow, Alaska (latitude $\sim 71^\circ N$) vary slightly by season; gradients are typically near zero in April and approximately 2–3‰ in October [Graven *et al.*, 2012]. Since previously observed spatial gradients in Northern Hemisphere background sites are not larger than the measurement uncertainty, uncertainty in Δ_{bg} is therefore expected to be similar to the measurement uncertainty of ± 2 ‰ or ~ 0.8 ppm. In previous work, β caused by respiration in California has been estimated to be 0.2 ± 0.1 ppm in 2009 [Turnbull *et al.*, 2011] and less than 0.5 ppm in 2004–2005 [Hsueh *et al.*, 2007]. This work assumes $\beta = 0.2 \pm 0.2$ ppm with a uniform magnitude and uncertainty over the state. Air-sea exchange is assumed to have a negligible effect on $\Delta^{14}C$ over California since air-sea gradients $\Delta^{14}C$ in the midlatitude Pacific are currently near zero [Graven *et al.*, 2012]. The uncertainty in background C_{bg} is estimated to be ~ 0.5 ppm based on sampling the NOAA East Pacific marine background CO_2 curtain in the same manner that Jeong *et al.* [2013] previously sampled background CH_4 .

Propagating the above uncertainties (which are dominated by uncertainty in measurement of $^{14}CO_2$) through equation (1) yields an uncertainty in $ffCO_2$ of ~ 1.3 ppm, which we round up to 1.5 ppm in this work. We note that this estimate is similar to uncertainties reported in recent studies by using flask measurements of CO_2 and $\Delta^{14}C$ in the Western U.S. (1.0–1.3 ppm, 1σ) [LaFranchi *et al.*, 2013; Turnbull *et al.*, 2011]. As described in the section on regional inversions, we conduct some sensitivity tests to estimate the effect of systematic offset and gain biases in estimated fossil fuel CO_2 .

2.1.2. OCO-2 Observations

NASA's OCO-2 satellite, launched in July 2014, was designed to provide global estimates of atmospheric CO_2 with the precision, resolution, and coverage needed to characterize sources and sinks on regional scales. Measurements of reflected sunlight (day time only) are made in the Oxygen-A band (0.76 μm) and the weak and strong CO_2 bands (1.6 and 2.06 μm , respectively), from which XCO_2 estimates are derived via an inverse retrieval algorithm. The OCO-2 mission collects nearly one million soundings per day (24 soundings/s) at approximately 3 km^2 nadir resolution [Crisp *et al.*, 2017]. After cloud and aerosol screening, approximately 20 to 30% (global average) of the total number of soundings remain for processing by the Level 2 retrieval algorithm [Taylor *et al.*, 2016]. The 233 orbit tracks in the NASA A-Train WRS-2 repeat cycle are spaced at approximately 1.55° longitude (~ 150 km at the equator). The nominal operation during the first year in space was to alternate between nadir and glint observing modes every 16 days (one complete repeat cycle). However, in July 2015, the nominal observation mode was updated to alternate between nadir and glint viewing on successive orbits, with some orbits that pass almost exclusively over oceans always in glint viewing mode. The ground tracks are highly repeatable and predictable, with approximately five orbits passing over parts of California.

For the time period analyzed here which was prior to the acquisition of real OCO-2 observations, synthetic OCO-2 soundings were generated by using the OCO-2 simulator at Colorado State University [O'Brien *et al.*, 2009]. These simulations were based on mission specifications in 2012 of collecting only four footprints per measurement frame. However, prior to launch, mission status doubled this to retrieve the full eight footprints per frame. The OCO-2 simulations included clouds and aerosols taken from a database of Cloud-Aerosol Lidar and Infrared Pathfinder Satellite Observation profile data [Winker *et al.*, 2010] and were screened by using a total optical depth threshold of 0.3. Simulations were run over a 32 day period in September and October to account for 16 day repeat cycles for nadir and glint viewing modes. We assume similar orbit tracks and data yield for inversion simulation experiments in November 2010 and May 2011, although we note that in reality, cloud coverage and glint orbits will shift during the year. These simplifications should have little bearing on the overall effects reported here.

To provide an initial estimate of the uncertainty in OCO-2 observations, we note that *Frankenberg et al.* [2015] reported that OCO-2 retrievals agreed with each other to within <0.5 ppm during thermal vacuum tests and here assume the random uncertainty in individual XCO_2 retrievals of 0.5 ppm for both local observations (over California) and for measurement of background inflow. Assuming that the random uncertainties in local and background measurements are uncorrelated, the difference measurement of local enhancement (local XCO_2 minus background XCO_2 difference) will have an uncertainty of $\sqrt{2} * 0.5$ ppm or ~ 0.7 ppm. For the inversion study described below, we also assume that individual retrievals are averaged into bins containing four retrievals on each ground track (equivalent to an $\sim 0.1^\circ$ on the ground) and that the random component of uncertainty in the binned data averages down by a factor of $(1/4)^{1/2} = 1/2$, from ~ 0.7 ppm to ~ 0.35 ppm.

We also note that the evaluation of systematic uncertainties in OCO-2 is currently unresolved and the subject of active research. To address this in a preliminary fashion, we also performed some sensitivity tests to systematic bias in XCO_2 . Here ongoing work suggests that bias corrections may range from <1 ppm to ~ 2 ppm, with potential (and as yet unquantified) uncertainties of $\sim 25\%$ (C. O'Dell, private communication, 2016). In this paper, we include a sensitivity test to a uniform 0.5 ppm offset in XCO_2 over California and evaluate the resulting changes in posterior estimates of fossil and biosphere CO_2 exchanges.

2.2. Prior Flux Models

2.2.1. Fossil Fuel Fluxes

In order to characterize the likely spatial and temporal variations of $ffCO_2$ emissions across California, we start with the Vulcan 2.2 emission map [*Gurney et al.*, 2009] as our primary $ffCO_2$ prior flux estimate and then estimate uncertainties by comparing Vulcan with other $ffCO_2$ emission data sets. Vulcan provides an hourly resolved fossil fuel CO_2 emission product on a $0.1 \times 0.1^\circ$ grid for 2002 that takes into account weekday and weekend variations in emissions from the location of power plants, roads, and industrial facilities including cement production. Even though we are focusing on the years 2010–2011, we use the Vulcan 2.2 product for the year 2002 without modification. We note that annual state total fossil fuel CO_2 emissions are estimated to have changed by less than 20% over the period 2002 to 2013 [CARB, 2015] such that the use of the 2002 inventory is unlikely to substantially affect our conclusions. We also use the Emission Database for Global Atmospheric Research (EDGAR, version FT2010) [*Emission Database for Global Atmospheric Research (EDGAR)*, 2011] $0.1 \times 0.1^\circ$ time-invariant emission map as an alternate $ffCO_2$ prior flux estimate (see section 2.5).

To approximate the regional uncertainty in prior fossil fuel emissions, we take two approaches. First we compare Vulcan with three other estimates of fossil fuel CO_2 emissions in California that are available as spatially distributed maps. The four emission maps: EDGAR (version FT2010) [EDGAR, 2011], Open-source Data Inventory for Anthropogenic CO_2 (ODIAC, version ODIAC2013a) [*Oda and Maksyutov*, 2011], Fossil Fuel Data Assimilation System (FFDAS, version 2.0) [*Asefi-Najafabady et al.*, 2014], and Vulcan [*Gurney et al.*, 2009], are shown in Figure 2. To provide a regionally specific estimate of prior fossil fuel emission uncertainty for use in the inversion, the regional and state total emission sums are compared in Table 2. Marine and aviation emissions are excluded from all inventories in this comparison, except for the gridded Vulcan emissions, which includes aviation emissions up to 3000 ft. In the air basin totals reported in Table 2, we have subtracted aviation emissions from Vulcan, which total 4.9 Tg C yr^{-1} across California. Cement emissions were included in all estimates except FFDAS, so for consistency, we added cement emissions from Vulcan to FFDAS in the air basin totals.

At the state scale, fossil fuel CO_2 emissions from ground-based sources (not including marine or aviation) in California estimated by Vulcan in 2002 are 87 Tg C yr^{-1} , while EDGAR, ODIAC, and FFDAS in 2008 are 104, 88, and 82 Tg C yr^{-1} , respectively. For comparison, the California Air Resources Board estimates statewide ground-based fossil fuel emission totals of 96, 94, and 90 Tg C yr^{-1} in 2002, 2008, and 2013, respectively [CARB, 2015], which is within the range of the four emission maps. The 1σ standard deviation in statewide total fossil fuel emissions in California across the four emission maps is $\sim 11\%$, equivalent to roughly 4 times the uncertainty (4–5% at 2σ) in total U.S. fossil fuel CO_2 emissions reported in previous synthesis studies [*Pacala et al.*, 2010; *Andres et al.*, 2014].

At the regional scale, we estimated the 1σ uncertainty in fossil fuel CO_2 emissions as the larger of the standard deviation of emissions across (1) the four emission maps or (2) the ensemble of FFDAS emission estimates in

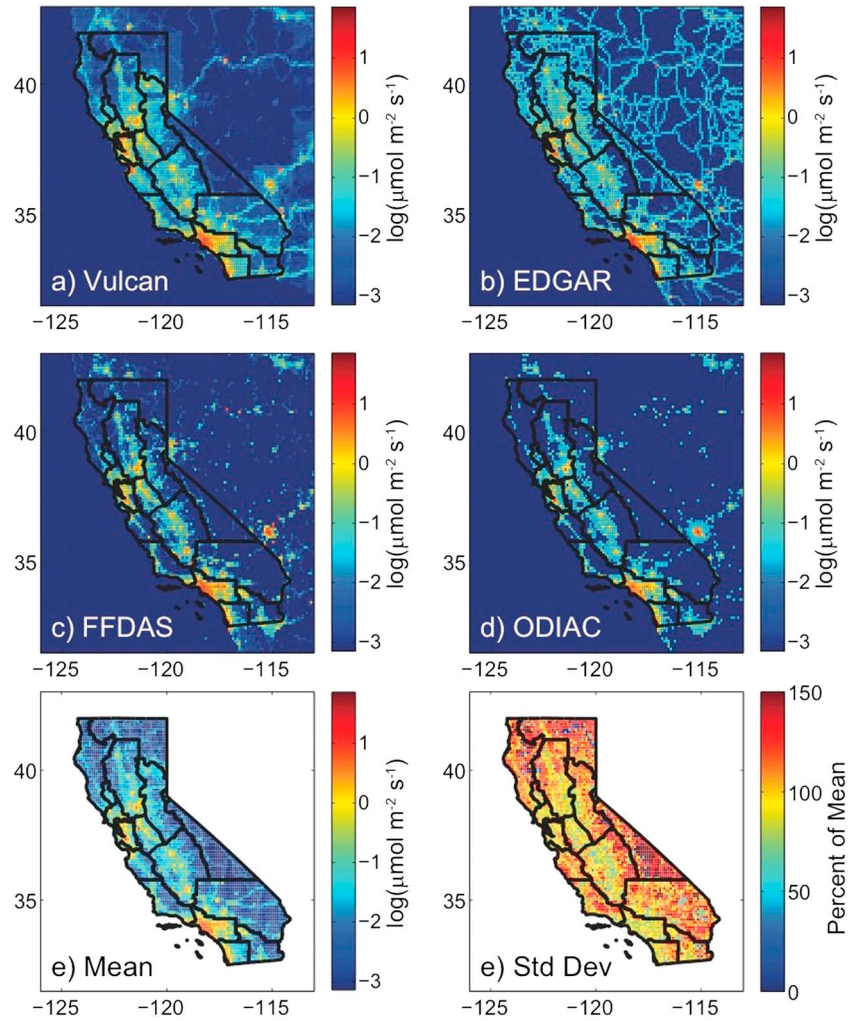


Figure 2. Annual mean fossil fuel CO₂ emissions in California from four gridded inventory products ($\log_{10}(\mu\text{mol m}^{-2} \text{s}^{-1})$): (a) Vulcan, (b) EDGAR, (c) FFDAS, and (d) ODIAC and (e) mean of four models and (f) standard deviation of four models.

Table 2. Summed Fossil Fuel Emissions in Individual Air Basins and Statewide Totals for Four Gridded Inventories, in Units of Tg C yr⁻¹

Region	Name	EDGAR	ODIAC 1 km	FFDAS	Vulcan
1	North Coast	1.6	0.5	0.5	1.0
2	Northeast Plateau	1.3	0.2	0.3	0.4
3	Sacramento Valley	7.4	6.2	6.4	6.8
4	Mountain Counties	2.1	0.8	0.8	2.2
5	Lake County	0.2	0.1	0.1	0.1
6	Great Basin Valleys	0.6	0.1	0.1	0.2
7	San Francisco Bay	17.5	12.1	11.1	16.4
8	San Joaquin Valley (North)	9.4	2.4	3.3	3.0
9	North Central Coast	2.2	2.0	1.5	6.0
10	Mojave Desert	4.3	4.4	4.5	6.1
11	South Central Coast	3.4	3.1	2.7	4.4
12	South Coast	35.5	33.8	31.2	26.9
13	Salton Sea	1.7	3.6	4.7	1.4
14	San Diego	6.6	6.4	6.9	6.6
15	Lake Tahoe	0.1	0.0	0.0	0.1
16	San Joaquin Valley (South)	10.8	12.3	8.6	5.6
	Total	104.7	88.0	82.7	86.9

Table 3. Prior Emissions (Tg C yr⁻¹) for ffCO₂ (Top) and bioCO₂ (Bottom) Exchanges in May and November^a

Region	1	2	3	4	5	6	7	8	9	10	11	12	13	14	15	16	Total
<i>May</i>																	
Fossil fuel	0.4	1.1	6.7	2.3	0.1	0.2	16.5	2.9	4.5	6.0	3.9	26.7	1.4	6.8	0.1	5.8	85.4
Biosphere	-3.0	-15.6	-17.0	-4.6	-1.7	0.2	-11.3	-6.1	-7.1	-5.1	-10.7	-5.9	-1.7	-4.5	0.3	-11.0	-104.8
<i>November</i>																	
Fossil fuel	0.4	1.0	6.8	2.2	0.1	0.3	17.5	3.0	5.1	6.2	3.9	25.9	1.3	6.5	0.1	5.7	86.0
Biosphere	7.2	14.3	9.1	5.5	1.5	2.2	9.7	5.8	9.3	1.4	8.8	1.9	0.1	0.3	0.2	15.0	92.3

^aNegative exchange refers to carbon uptake by the land surface.

Asefi-Najafabady et al. [2014]. Generally speaking, the largest emissions are obtained in the largest metropolitan regions (i.e., South Coast, San Francisco Bay, and San Diego), with substantial emissions also from the Sacramento and San Joaquin Valley. For most regions, the standard deviation across the four emission maps, corresponding to fractional deviations between 10% and 74%, was larger than the standard deviation across the FFDAS ensemble. However, the standard deviation across the four emissions maps for San Diego was smaller (4%) than the standard deviation across the FFDAS ensemble (10%), so we used the larger FFDAS-based estimate to specify uncertainty in San Diego. The estimated mean prior ffCO₂

Table 4. Prior and Posterior Emission Uncertainties for Fossil Fuel and Biosphere CO₂ Exchange in May and November^a

Region	1	2	3	4	5	6	7	8	9	10	11	12	13	14	15	16
<i>May</i>																
Fossil fuel																
Prior	1.07	0.59	0.10	0.52	0.40	0.95	0.23	0.74	0.77	0.22	0.19	0.10	0.57	0.10	1.15	0.31
Post.OCO2	1.07	0.57	0.10	0.52	0.40	0.53	0.23	0.71	0.77	0.22	0.18	0.10	0.57	0.10	1.13	0.30
Post.Flask	1.07	0.57	0.09	0.51	0.40	0.95	0.06	0.66	0.69	0.20	0.19	0.04	0.57	0.07	1.15	0.18
Post.OCO2 + Flask	1.07	0.53	0.09	0.51	0.40	0.49	0.06	0.63	0.69	0.20	0.18	0.04	0.56	0.07	1.13	0.18
Post.100%.prior.err	1.00	0.79	0.16	0.95	1.00	0.55	0.06	0.81	0.85	0.41	0.45	0.05	0.97	0.09	0.98	0.23
Post.Rflask = 0.75	1.07	0.54	0.09	0.51	0.40	0.50	0.07	0.65	0.72	0.21	0.18	0.06	0.57	0.08	1.13	0.21
Post.ffCO2.only	1.07	0.59	0.10	0.52	0.40	0.95	0.12	0.72	0.75	0.21	0.19	0.06	0.57	0.08	1.15	0.25
Biosphere																
Prior	0.47	0.51	1.02	0.45	0.75	2.61	1.35	1.08	0.66	0.36	1.00	1.04	0.27	0.81	3.13	0.78
Post.OCO2	0.34	0.31	0.57	0.44	0.75	1.03	1.00	0.95	0.59	0.34	0.85	1.03	0.27	0.81	1.21	0.37
Post.Flask	0.20	0.05	0.06	0.34	0.31	1.40	0.04	0.39	0.44	0.23	0.24	0.19	0.27	0.73	2.12	0.09
Post.OCO2 + Flask	0.16	0.05	0.06	0.33	0.31	0.80	0.04	0.38	0.41	0.22	0.23	0.19	0.27	0.73	1.09	0.09
Post.100%.prior.err	0.18	0.05	0.06	0.44	0.33	0.65	0.04	0.39	0.47	0.28	0.24	0.19	1.00	0.88	0.76	0.09
Post.Rflask = 0.75	0.20	0.06	0.08	0.37	0.40	0.87	0.05	0.50	0.48	0.27	0.30	0.28	0.27	0.77	1.13	0.12
<i>November</i>																
Fossil fuel																
Prior	1.07	0.59	0.10	0.52	0.40	0.95	0.23	0.74	0.77	0.22	0.19	0.10	0.57	0.10	1.15	0.31
Post.OCO2	1.07	0.59	0.10	0.52	0.40	0.58	0.23	0.66	0.76	0.22	0.19	0.10	0.55	0.10	1.12	0.31
Post.Flask	1.06	0.52	0.09	0.48	0.40	0.95	0.07	0.50	0.72	0.20	0.19	0.06	0.57	0.07	1.15	0.17
Post.OCO2 + Flask	1.06	0.52	0.09	0.48	0.40	0.52	0.07	0.48	0.71	0.20	0.18	0.06	0.55	0.07	1.12	0.17
Post.100%.prior.err	1.00	0.73	0.20	0.83	1.00	0.67	0.08	0.58	0.88	0.46	0.55	0.07	0.91	0.09	0.98	0.21
Post.Rflask = 0.75	1.06	0.54	0.09	0.49	0.40	0.54	0.09	0.53	0.73	0.21	0.18	0.07	0.55	0.08	1.12	0.20
Post.ffCO2.only	1.07	0.57	0.09	0.50	0.40	0.95	0.08	0.56	0.73	0.21	0.19	0.07	0.57	0.08	1.15	0.18
Biosphere																
Prior	0.71	0.24	0.66	0.72	0.13	0.17	0.40	0.21	0.61	0.48	1.90	1.82	1.14	1.28	0.60	0.78
Post.OCO2	0.61	0.23	0.58	0.71	0.13	0.17	0.39	0.20	0.60	0.47	1.61	1.81	1.13	1.27	0.52	0.70
Post.Flask	0.24	0.02	0.16	0.49	0.13	0.17	0.22	0.17	0.58	0.45	0.98	0.54	1.11	0.77	0.60	0.23
Post.OCO2 + Flask	0.23	0.02	0.16	0.49	0.13	0.17	0.22	0.17	0.57	0.44	0.91	0.54	1.10	0.76	0.51	0.22
Post.100%.prior.err	0.25	0.02	0.17	0.59	0.79	0.76	0.26	0.28	0.86	0.75	0.75	0.50	0.97	0.69	0.70	0.23
Post.Rflask = 0.75	0.30	0.03	0.22	0.57	0.13	0.17	0.27	0.18	0.59	0.45	1.12	0.75	1.12	0.94	0.51	0.30

^aValues are presented as fractions of prior emissions from Table 3. Posterior results are presented for inversions by using prior uncertainties with only OCO-2 observations (Post.OCO2), only flask observations (Post.Flask), and OCO-2 and flask observations together (Post.OCO2 + Flask). Results for sensitivity tests using 100% prior uncertainties for fossil and biosphere exchanges (Post.100%.prior.err), 75% model measurement uncertainty for flask observations (Post.Rflask = 0.75), and an inversion of fossil fuel emissions by using only flask ¹⁴CO₂ observations (Post.ffCO2.only) are also shown.

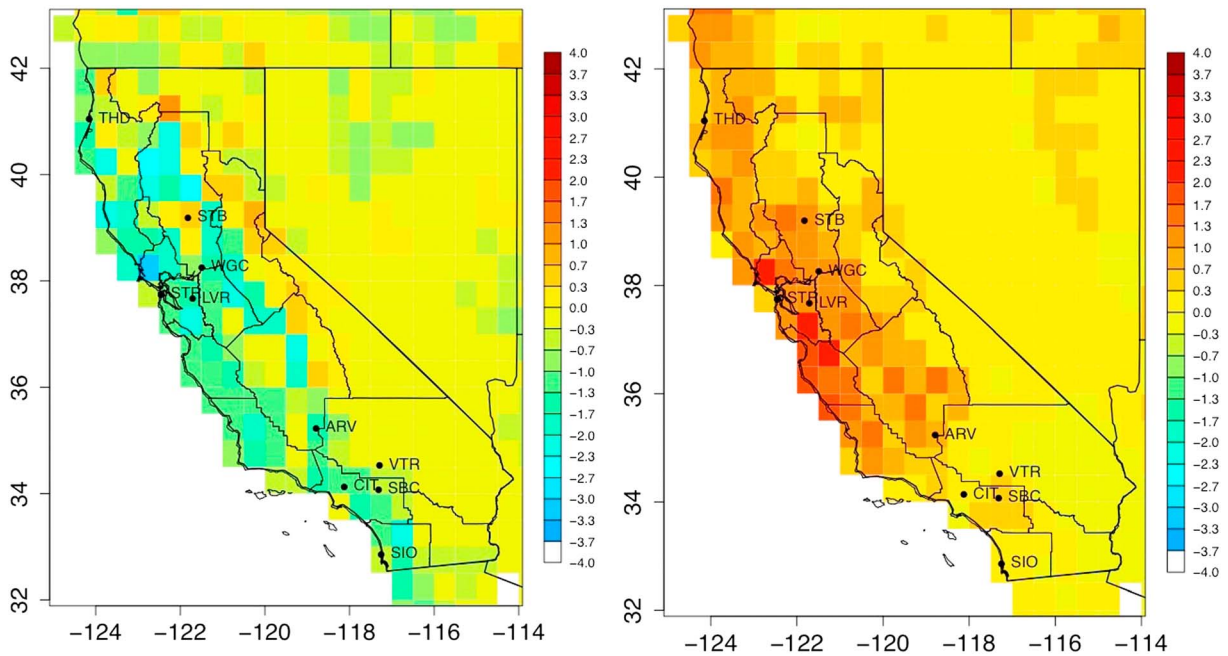


Figure 3. CASA net ecosystem CO_2 exchange ($\mu\text{mol m}^{-2} \text{s}^{-1}$) for (left) May and (right) November with sampling sites and air basin regions. Positive exchange is oriented to the atmosphere.

emissions for the two seasons (May and November) differ slightly from the annual mean and are shown in Table 3, while the fractional uncertainties in prior regional emissions are shown in Table 4 (together with prior biosphere and posterior uncertainty estimates described later in this paper).

2.2.2. Terrestrial Biosphere Fluxes

We prescribe net biosphere CO_2 fluxes by using the Carnegie Ames Stanford Approach (CASA) Global Fire Emissions Database Version 3 model with $0.5 \times 0.5^\circ$ resolution [van der Werf *et al.*, 2010] adapted for the NASA Carbon Monitoring System (CMS) Flux Pilot Project (<http://cmsflux.jpl.nasa.gov/>). The model employs remotely sensed meteorology together with vegetation index from Moderate Resolution Imaging Spectroradiometer (MODIS) and an estimated light use efficiency parameterization to simulate net primary productivity and a soil model to simulate heterotrophic respiration and thereby net ecosystem production [Collatz *et al.*, 2013]. In this implementation, we imposed the diurnal cycle from the $1.25 \times 1.0^\circ$ fluxes onto the nearest neighbor $0.5 \times 0.5^\circ$ monthly mean fluxes to approximate hourly resolved biosphere fluxes at 0.5° resolution. Estimated monthly mean fluxes are shown for the California domain in Figure 3. Summing over land surface emissions yields prior estimates of bio CO_2 exchange for the 16 regions of California shown in Table 3, with state totals of -104 and 91 Tg C yr^{-1} for May and November, respectively (where positive emissions are oriented toward the atmosphere). Here we note that the large variation in seasonal net biosphere carbon exchange poses a challenge for assessment of the net annual exchange. Estimating the net annual source or sink of CO_2 in California would require year-round observations, but we do not explicitly address net annual exchanges in the current study.

Prior uncertainty in biosphere CO_2 exchange was estimated by combining two approaches. First, we applied estimated uncertainties derived from a sensitivity analysis of net ecosystem exchange to CASA model parameters, sampling populations of values normally distributed around baseline values [Liu *et al.*, 2014]. Standard deviation values were based on literature reviews (NPP, Q10, and wood mortality), reported data uncertainty (e.g., woody cover fraction is a MODIS product reported to have 10% uncertainty), and expert opinion (for the heterotrophic response to soil moisture). Summing these uncertainties in quadrature over the air basins, fractional uncertainties range from 10 to 200%, depending on region and season. For a subset of regions exhibiting what we considered small uncertainty ($<20\%$), we compared emissions with those estimated from CarbonTracker (Carbon Tracker, 2013, [ftp://aftp.cmdl.noaa.gov/products/carbontracker/co2/fluxes/monthly/;version 2013B](ftp://aftp.cmdl.noaa.gov/products/carbontracker/co2/fluxes/monthly/;version%202013B)) assimilations for the corresponding dates and used the fractional difference

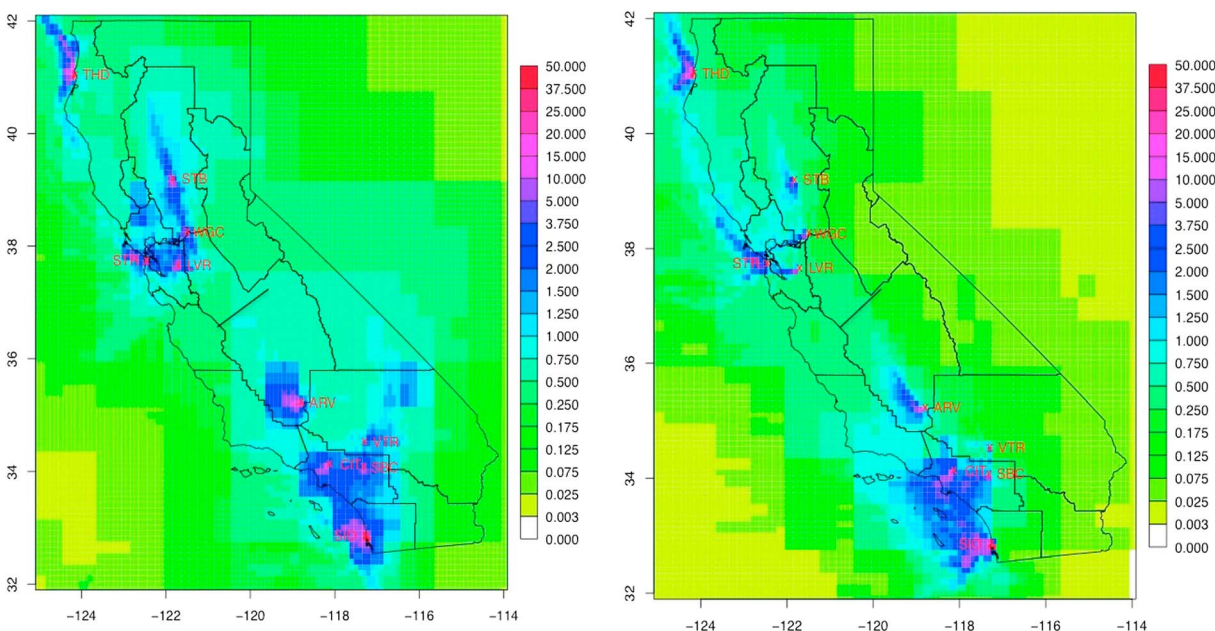


Figure 4. WRF-STILT footprints ($\text{ppm}/\mu\text{mol m}^{-2} \text{s}^{-1}$) for tower flask sampling sites, showing mean sensitivity to surface emissions at 2200 UT local time for the months of May and November.

between CASA and CarbonTracker for those regions. The resulting estimated fractional uncertainties are reported in Table 4. For the purposes of this analysis, we assume that the resulting uncertainties between different regions are uncorrelated, but note that this assumption could be revisited in future work.

2.3. Atmospheric Transport and CO₂ Signal Prediction

We apply the Coupled Weather Research and Forecasting/Stochastic Time-Inverted Lagrangian Transport (WRF-STILT) model [Lin et al., 2003; Nehrkorn et al., 2010] to compute transport meteorology and footprint predictions for May 2011 and November, 2010. WRF version 3.5.1 is used to simulate meteorology in domains covering western North America at 36 and 12 km, nesting down over subregions of California at 4, and 1.3 km resolutions following work described in Jeong et al. [2013]. As in Jeong et al. [2013], we use the five-layer thermal diffusion land surface model for May when irrigation provides an additional source of land surface moisture in California, and the Noah land surface model for November. To compute CO₂ measurement sensitivity to surface fluxes (footprints) from hourly WRF outputs, an ensemble of 500 STILT particles are released from each receptor and run backward in time for 7 days driven with meteorology from WRF output. In the case of OCO-2 receptors, 500 particles are released along nadir vertical columns and distributed across 10 vertical layers of 1 km thickness from the land surface to the top layer of the WRF model atmosphere of 10 km altitude, corresponding to ~75% of the atmospheric column. The density of particles per layer varies in proportion to the mean layer pressure along the column to approximate the column profile. While this approach does not include a more detailed representation of the OCO-2 observation profile, it is unlikely to strongly affect the results. Figure 4 shows monthly mean footprints for the flask receptors at 2200 UT, when flasks would be collected. In general, footprint sensitivity is largest near the receptor sites and tracks the upwind direction backward in time. For each site and time point, the simulated hourly resolved CO₂ signals were calculated by summing over the footprint times the corresponding flux over each of the 16 regions within California and remaining land surface fluxes in the modeling domain outside California for a 17th region. We use the term signal to refer to the local enhancement or depletion in CO₂ concentration caused by fossil fuel emissions or biospheric exchange occurring within our domain. In this work we do not explicitly estimate background CO₂ variations from outside the model domain but do include an approximate estimate of uncertainty due to CO₂ background as described above.

Following previous work we include estimated uncertainties in predicted CO₂ signals due to uncertainties in modeled atmospheric transport, planetary boundary layer (PBL) and wind velocities, limited numbers of particles, and background subtraction [e.g., Lin et al., 2003; Göckede et al., 2010]. Applying these techniques to

California, previous studies compared WRF-STILT predictions with data from radar wind profilers located across California to estimate uncertainty in predicted CH₄ signals due to errors from modeled PBL heights and winds in the WRF-STILT model. Resulting 68% confidence level (CL) uncertainties in predicted CH₄ signals ranged from 0.3 to 0.8 times the mean monthly signals [e.g., Jeong *et al.*, 2013]. Here we assume 68% CL transport model uncertainty of 0.5 times the magnitude of the mean monthly local CO₂ signal for each site for flask measurements and 0.3 times monthly XCO₂ signals for OCO-2 because the XCO₂ is not as sensitive to uncertainty in predicted planetary boundary layer depth as the tower measurements. As described in section 2.4 below, we conduct a sensitivity analysis to quantify the effect of biases in flask and OCO-2 observations.

2.4. Inversion Method

The scaling factor Bayesian inversion method relates model predictions to measurements as

$$\mathbf{c} = \mathbf{K}\lambda + \mathbf{v}, \quad (3)$$

where \mathbf{c} is the observed background-subtracted measured mixing ratios, \mathbf{K} is a matrix representing predicted mixing ratios for each region as the summed product of footprint \mathbf{F} and prior flux \mathbf{f} (i.e., $\mathbf{K} = \mathbf{F}\mathbf{f}$), λ is a vector of scaling factors for the CO₂ exchange from each of the spatial regions across California, and \mathbf{v} is a model-data mismatch vector with covariance matrix \mathbf{R} . Here \mathbf{R} is represented as a diagonal matrix representing the total uncertainty contributed by all sources of uncertainty (e.g., measurement and transport) summed in quadrature. Under the assumption of normally distributed (Gaussian) uncertainties, the posterior estimates for λ can be solved as

$$\lambda_{\text{post}} = (\mathbf{K}^T \mathbf{R}^{-1} \mathbf{K} + \mathbf{Q}_i^{-1})^{-1} (\mathbf{K}^T \mathbf{R}^{-1} \mathbf{c} + \mathbf{Q}_i^{-1} \lambda_{\text{prior}}), \quad (4)$$

where λ_{prior} is the separate prior flux estimate for fossil fuel and biospheric fluxes from the 16 air basins in California plus one region representing fluxes from outside California and the superscript “ T ” and “ -1 ” indicate the matrix transpose and inverse, respectively. Since we take the scaling factor approach, λ_{prior} is specified to be unity and \mathbf{Q}_i is the uncertainty covariance matrix representing prior model uncertainties in fossil fuel and biospheric fluxes. Again, under the assumption of normally distributed uncertainties, the posterior error covariance for λ can be written as

$$\mathbf{V}_{\text{post}} = (\mathbf{K}^T \mathbf{R}^{-1} \mathbf{K} + \mathbf{Q}_i^{-1})^{-1}. \quad (5)$$

2.5. Inversions Using Simulated Data

To estimate how much the posterior uncertainty in regional ffCO₂ and bioCO₂ exchanges is reduced relative to the prior uncertainties through inversions by using simulated data, we computed posterior exchanges and their uncertainties for each region for May and November. Here posterior fluxes are the product of the prior exchanges and the posterior scaling factors λ_{post} from equation (4). Posterior uncertainties in regional exchanges are the product of prior exchanges and the uncertainty in posterior scaling factors given by the square root of \mathbf{V}_{post} in equation (5). In this implementation, flask measurements are assumed to provide direct measures of both total CO₂ and ffCO₂ (from radiocarbon), while OCO-2 spatially binned column measurements provide total CO₂. This generates measurement matrices with ~150 flask measurements of ffCO₂ and of total CO₂ (10 sites each sampled every other day for a month) and a roughly equal number of spatially binned OCO-2 total-column CO₂ observations per month. The exchange estimates comprise 34 values of λ , corresponding to ffCO₂ and bioCO₂ exchanges for the 16 regions inside California and a 17th region representing signals from the remainder of the model domain outside California.

We estimate the reduction in posterior uncertainties for ffCO₂ and bioCO₂ exchanges from each region of California for three observation strategies: (a) only using OCO-2 measurements of total CO₂ = ffCO₂ and bioCO₂; (b) only using flask measurements that include both ffCO₂ and total CO₂; and (c) using OCO-2 measurements of total CO₂ and flask measurements of both ffCO₂ and total CO₂. For each case, we compute the 34 posterior scaling factors and their uncertainties for ffCO₂ and bioCO₂ exchange in the 17 regions. We then estimate the uncertainty in statewide California exchange, σ_E , for fossil fuel or biosphere CO₂ exchange including error correlations as

$$\sigma_E^2 = \mathbf{E}_{\text{prior}} \mathbf{V}_{\text{post}} \mathbf{E}_{\text{prior}}^T, \quad (6)$$

where $\mathbf{E}_{\text{prior}}$ is a vector of regional fossil fuel or biosphere CO₂ exchange.

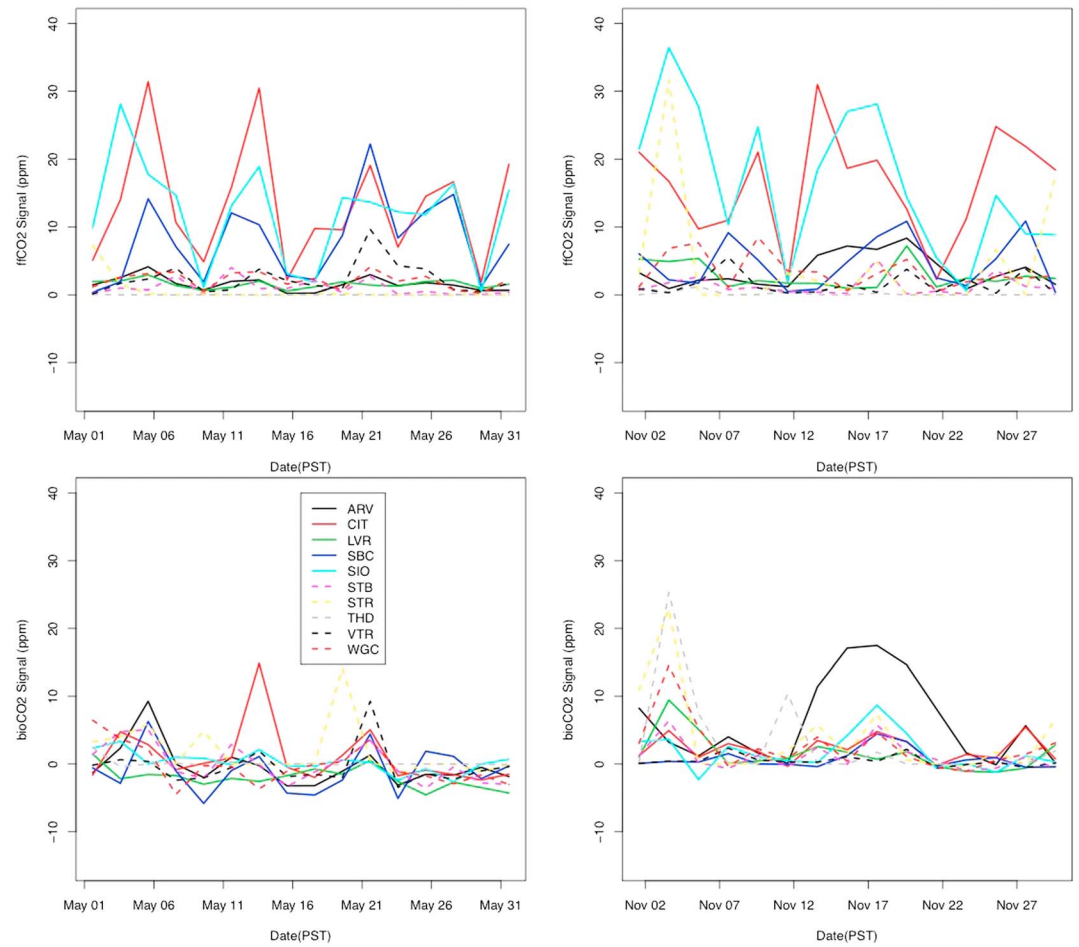


Figure 5. Predicted synthetic prior CO₂ mixing ratio (ppm) signals for (top row) fossil fuel and (bottom row) biosphere exchanges for flasks sampled at 2200 UT (1400 PST) for each tower site for months of (left column) May and (right column) November.

2.6. Sensitivity Tests for Random and Systematic Errors

In addition to the above, we also performed some sensitivity tests varying the assumptions of random uncertainties. First, we tested the power of the observational data to constrain posterior emissions under the assumption that emissions from all regions are poorly known by increasing the prior flux uncertainty to 100% in all regions. Second, we tested how much the posterior emission uncertainties changed in response to an increase in assumed model-measurement uncertainty (e.g., due to increased atmospheric transport model uncertainty) by increasing the signal-dependent scaling of the **R** matrix for the tower observations from 0.5 to 0.75 of the mean monthly signal for the tower sites. We do not change the model-measurement uncertainty for OCO-2, which has the effect of allowing for higher uncertainty in surface level transport and planetary boundary layer depth. Third, we tested whether the reductions in posterior uncertainty for ffCO₂ obtained from flasks alone are affected by the concurrent inversion of bioCO₂ exchanges by comparing posterior uncertainties obtained above to an inversion using flask measurements of ffCO₂ only to determine ffCO₂ emissions.

Next, we examine the sensitivity of inversions for ffCO₂ emissions alone to the use of an incorrect prior model for ffCO₂ emissions. Here we effectively test whether the tower network can recover “true” emissions calculated by using Vulcan emissions if “incorrect” prior signals are calculated by using an alternate emission model. For this test, we perform an inversion by using observed “true” signals computed with Vulcan and “incorrect” prior signals computed with either the EDGAR map or a spatially uniform map with flux = 1 μmol m⁻² s⁻¹. In both cases, the uncertainties in prior emissions are estimated as the absolute difference of prior minus Vulcan emissions for each region. We then examine the posterior emissions by

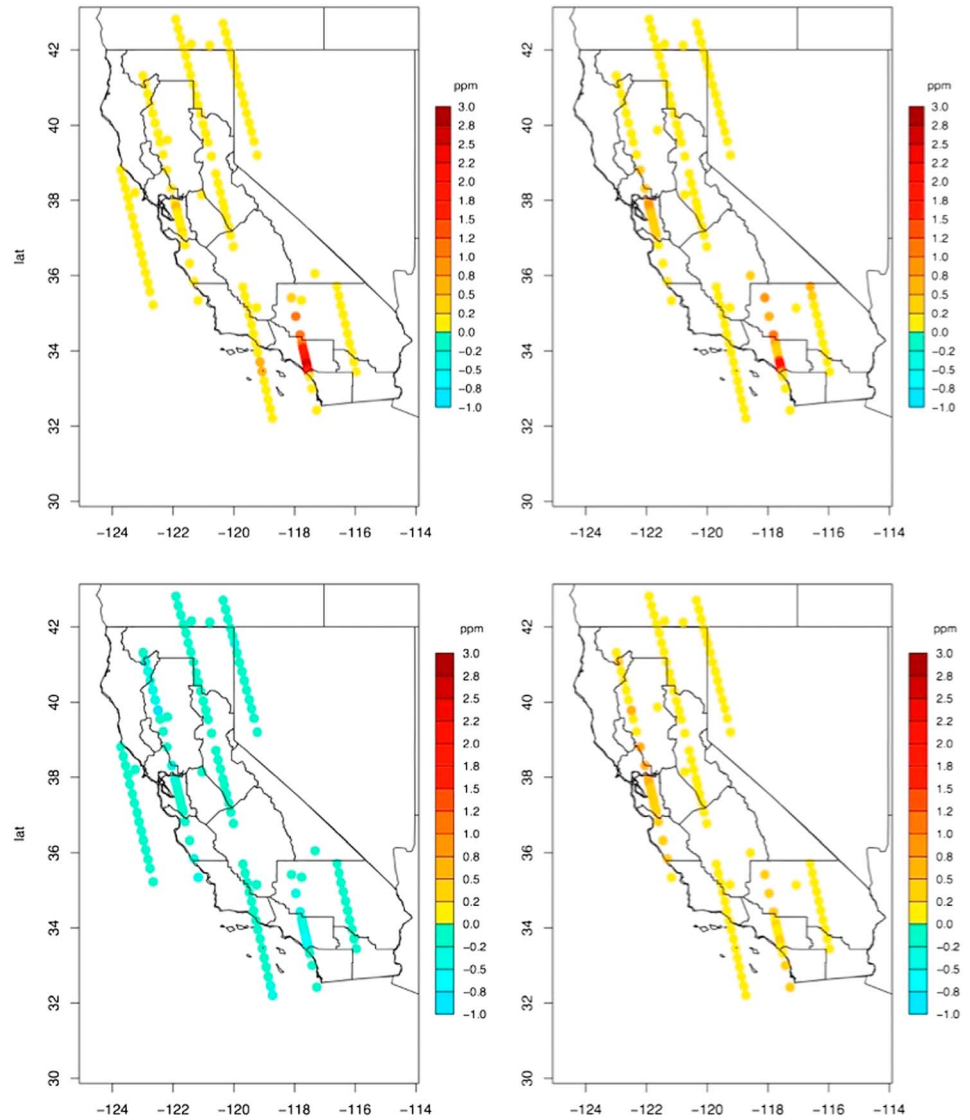


Figure 6. Predicted (top row) fFCO₂ and (bottom row) bioCO₂ column mean mixing ratio signals (ppm) for OCO-2 nadir overpasses for (left column) May and (right column) November. Predicted column retrievals have been averaged into approximately 0.1° bins (four retrievals per bin) along each track as used in the inversions.

region to identify how well the inversion recovers the “correct” (Vulcan) emissions by region and for the state total.

Last, we also conducted sensitivity tests to explore the effect of systematic biases in the models and/or observations. Here we tested the effect of a systematic 10% underestimate in the strength of predicted signals (e.g., due to systematic bias in PBL depth) and uniform +0.5 ppm offset biases in either the flask or OCO-2 observations (e.g., due to systematic bias in background CO₂). While these tests are not comprehensive, they provide insight into the impacts of possible biases on posterior fFCO₂ and bioCO₂ exchanges.

3. Results

3.1. Simulated fFCO₂ and BioCO₂ Observations

Simulated fFCO₂, bioCO₂, and total CO₂ observations were computed for flask and OCO-2 receptors over each monthlong period. Time series of monthly flask measurements are shown in Figure 5 for the 10 tower sites. In urban areas, simulated fFCO₂ signals are typically larger than bioCO₂ signals ($|\text{bioCO}_2/\text{fFCO}_2| < 0.1\text{--}0.2$). The fFCO₂ signals sometimes reach levels of 5–30 ppm in the urban areas of southern California (CIT, SBC, and

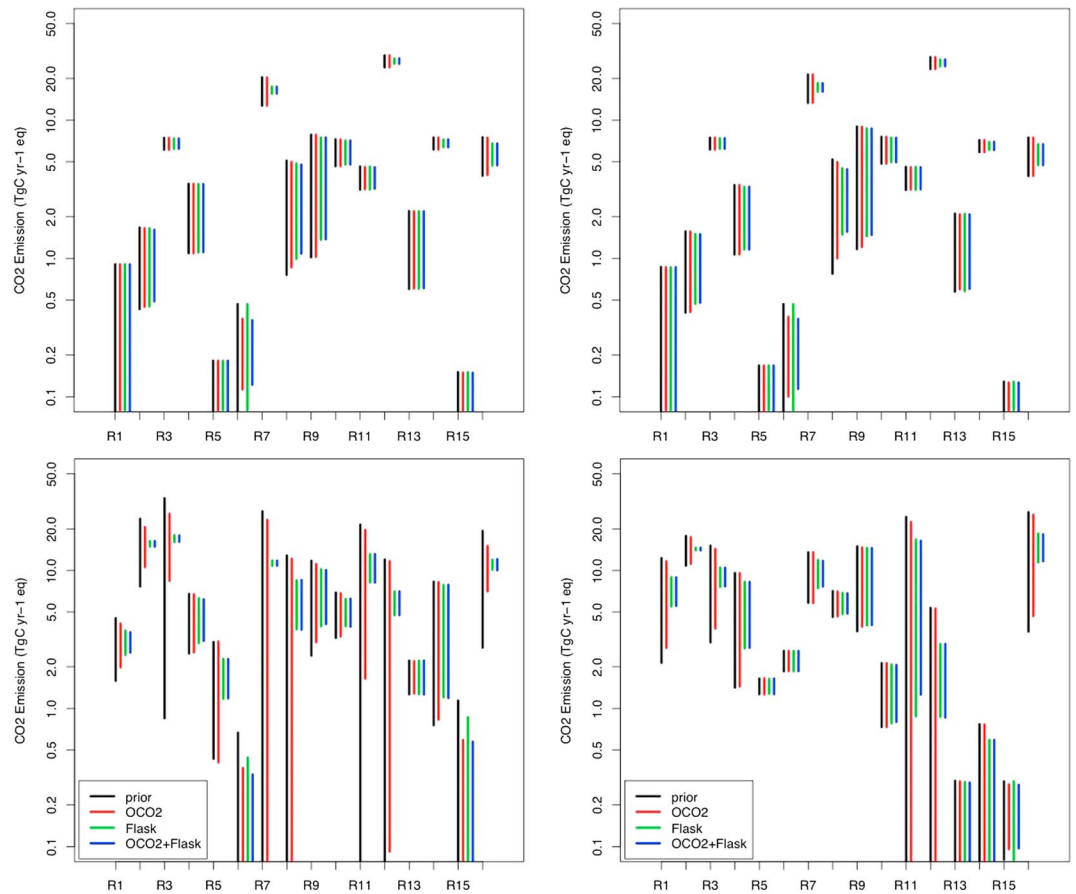


Figure 7. Estimated prior and posterior emissions in (top row) $ffCO_2$ and (bottom row) biosphere exchange for different CA air basins in months of (left column) May and (right column) November. Line lengths indicate uncertainties in prior (black) and posterior estimates obtained by using OCO-2 alone (red), flask observations alone (green), and OCO-2 and flasks together (blue). Note that May biosphere exchanges ($Tg\ C\ yr^{-1}\ eq$) are negative, though all scales are logarithmic to show fractional variations in uncertainties. Regions with the combination of CO_2 exchange and footprint sensitivity show significant reduction in posterior uncertainties for $ffCO_2$ emissions (e.g., 3 = Sacramento Valley, 7 = SF Bay, 12 = SoCAB) and biosphere exchange (2 = North Coast, 3 = Sacramento Valley, 12 = SoCAB, 16 = San Joaquin Valley).

SIO), similar to observations by *Newman et al.* [2013]. The simulations suggest that $ffCO_2$ is weaker in San Bernardino and stronger in San Diego in November, relative to May, due to seasonal changes in the meteorology. In suburban and rural areas, $bioCO_2$ signals ($\sim 1-10\ ppm$) are generally comparable to or larger than $ffCO_2$ signals ($|bioCO_2/ffCO_2| \sim 0.8-2$). Here $bioCO_2$ signals are sometimes negative (indicating net CO_2 drawdown) at some sites and sample dates in May, though some are positive, indicating that the contribution from respiration exceeds that from photosynthesis. In November, $bioCO_2$ signals are generally positive because respiratory fluxes dominate. The resulting $ffCO_2$ and $bioCO_2$ signals can often be large compared to the measurement uncertainties. In these cases, the estimated transport model uncertainties (which are proportional to the mean monthly signal) tend to dominate the model-data uncertainty for the flask samples.

Figure 6 shows the predicted $ffCO_2$ and $bioCO_2$ signals for the spatially binned XCO_2 signals for OCO-2 along the nominal nadir observation tracks. In general, the simulated $bioCO_2$ and $ffCO_2$ in XCO_2 is comparable to or smaller than the measurement uncertainty assumed for the spatially binned OCO-2 measurements (0.35 ppm). The exception is in or near major urban areas where $ffCO_2$ signals are 1–2 ppm and in some rural areas where $bioCO_2$ signals approach or exceed 1 ppm.

Here we note that CO_2 signals from outside California effectively add a random noise to the observations because the transport model error is assumed to be proportional to the mean signal level as described

Table 5. Summary of California State Total Posterior Emission Uncertainties as a Fraction of Statewide Prior Emissions (From Table 3) for Fossil (Sum.ff) and Biosphere (Sum.bio) CO₂ Exchange

	Sum.ff	Sum.bio
<i>May</i>		
Prior	0.081	0.288
Post.OCO2	0.080	0.220
Post.Flask	0.048	0.055
Post.OCO2 + Flask	0.048	0.053
Post.100%.prior.err	0.067	0.062
Post.Rflask = 0.75	0.053	0.064
Post.ffCO2.only	0.060	
<i>November</i>		
Prior	0.084	0.258
Post.OCO2	0.083	0.222
Post.Flask	0.054	0.095
Post.OCO2 + Flask	0.053	0.092
Post.100%.prior.err	0.072	0.073
Post.Rflask = 0.75	0.058	0.114
Post.ffCO2.only	0.057	

above. For the tower observations, predicted CO₂ signals from outside California (not shown) are small compared to the total signal from within California for most flask sites (<10%), except for Trinidad Head, where they can be ~30–100% of the California signal when northerly winds transport bioCO₂ signals from the northwest U.S. and Canada. For most OCO-2 observations, signals outside California are roughly equivalent to signals inside California because of the larger spatial footprints.

3.2. Posterior Estimates and Uncertainty Reductions

As described in section 2.5, we first estimate the reduction in posterior

uncertainty relative to the prior that is obtained by applying equation (5), using predicted signals and the baseline assumptions regarding prior and model-measurement uncertainties. Here we compare results obtained with OCO-2, flask, and OCO-2 and flask data together to provide constraints on the combination of fossil fuel and biospheric CO₂ exchanges (Figure 7). Figure 7 and Table 4 show the fractional posterior uncertainties in fossil fuel and biosphere CO₂ exchange by region. In general, significant reductions below prior fossil fuel emission uncertainties are obtained for the San Francisco Bay Area, the South Coast Air Basin, San Diego, and the Southern San Joaquin Valley (regions 7, 12, 14, and 16) by using the flask data, while posterior uncertainty in the Sacramento urban area (region 3) is not significantly different than the already small (10%) prior uncertainty. Posterior uncertainty is similar to the prior uncertainty in other regions (e.g., 4, 6, and 13) because of either the lack of towers or small ffCO₂ emissions from those regions.

Using simulated OCO-2 observations alone, we find an influence on posterior ffCO₂ emission uncertainties in region 6, but the 16-day repeat swaths do not overlap strongly with urban regions containing large emissions. For biosphere exchange, detectable reductions in uncertainty are found for several regions with OCO-2 (e.g., region 1, 2, 3, 6, 8, 9, 15, and 16) and nearly all regions (except 13) with flasks in May. The effect of the inversion is smaller in November when fluxes are weaker and generally positive with respect to the atmosphere due to respiration overwhelming photosynthesis. The stronger constraint on bioCO₂ as compared to ffCO₂ is likely due in part to the large prior uncertainty relative to ffCO₂ and/or stronger exchange (e.g., region 3).

The statewide prior and posterior uncertainties are shown in Table 5. For the cases including flask observations, statewide ffCO₂ emission uncertainties are reduced from 8.1% and 8.4% to 4.8% and 5.3% in May and November, respectively, primarily due to the constraints of flask data on the strongly emitting regions of San Francisco Bay Area, the South Coast Air Basin, San Diego, and the Southern San Joaquin Valley. State total uncertainty in biosphere CO₂ exchange is reduced from 29% and 26% to 5.3% and 9.2% in May and November, respectively. In the above cases, OCO-2 observations alone produce little reduction in posterior ffCO₂ uncertainties but a finite reduction in posterior bioCO₂ uncertainties when estimated without tower observations (from 29 to 20% and from 26% to 22%, in May and November, respectively). Here we note that the cross correlations in posterior uncertainties are generally found to be small and negative, reducing the uncertainty in statewide CO₂ exchange from 0 to ~10% below that obtained assuming uncorrelated posterior errors.

3.3. Sensitivity Tests for Random Errors

As described above, we also conducted sensitivity tests for random uncertainties and systematic biases. First, we tested how much the observations reduced emission uncertainties in a case with large (100%) prior

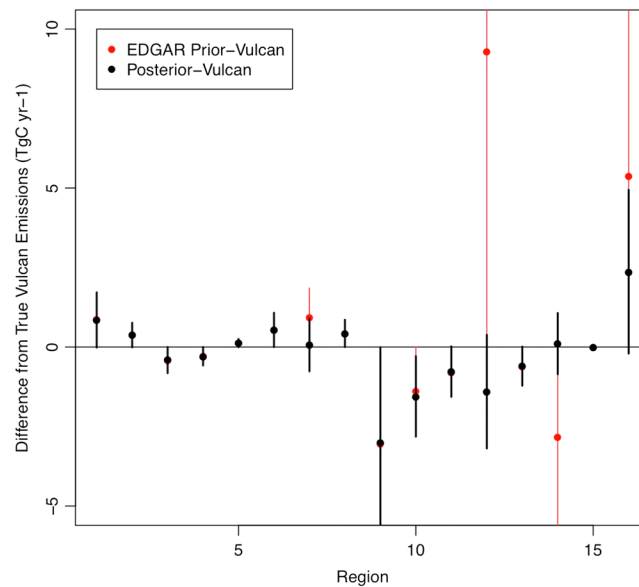


Figure 8. Differences from regionally summed “true” Vulcan ffCO₂ emissions for “incorrect” prior emissions (Tg C yr⁻¹) calculated by using EDGAR (red) and resulting posterior emission estimates obtained from the inversion (black) by using flask observations ¹⁴CO₂. The error bars represent prior and posterior uncertainties, respectively.

in many regions (i.e., 1, 2, 3, 7, 8, 9, 10, 11, 12, 14, and 16) in May, though fewer (i.e., 3, 7, 12, and 16) in November, lowering the uncertainties in California total bioCO₂ from prior estimates of 32% and 33% to posterior estimates of 6.2% and 7.3% in May and November, respectively. This suggests that regionally summed ffCO₂ (bioCO₂) emissions could be estimated to within 6–7% in May and November even with poorly known prior emissions, provided that the assumptions regarding model-measurement uncertainties are valid.

Second, we increased the uncertainties in the component of the model-measurement error due to transport model uncertainty in the flask observations, increasing the measurement uncertainty from 0.5 to 0.75 of the mean signal strength for each site with flask observations. Not surprisingly, we found that the posterior uncertainties did not change for regions where uncertainties due to transport model uncertainty were small compared to flask ffCO₂ measurement uncertainty (e.g., regions 6 and 15) but did increase roughly 25% in regions where uncertainties due to transport error were large (e.g., regions 7 and 12). However, resulting posterior uncertainties in California total ffCO₂ emissions were 5.3% in May and 5.8% in November and 6.4% and 11.4% in bioCO₂ exchange in May and November, respectively, increasing only slightly because the regional uncertainties were summed in quadrature and many of the other posterior uncertainties were largely unchanged.

Third, we estimated the reduction in uncertainty for ffCO₂ emissions obtained by using only the flask-based measurements of ¹⁴CO₂. Here the uncertainties were reduced for several regions (7, 12, 14, and 16) where signals are large compared to measurement uncertainty as shown in Figure 8. Summing across regions, the uncertainty in California total ffCO₂ emissions again was reduced to ~6%, only slightly larger than that found by using both ffCO₂ and total CO₂ measurements to simultaneously estimate ffCO₂ and bioCO₂. This suggests that much of the reduction in posterior estimates of ffCO₂ are obtained from the radiocarbon measurements.

3.4. Sensitivity Tests for Systematic Errors

First, we tested the effect of applying incorrect prior maps for ffCO₂ emissions. Here we first used the “true” Vulcan ffCO₂ emission map to compute the simulated flask observations and used “incorrect” EDGAR ffCO₂ emissions to compute prior signals, with prior uncertainties in emissions estimated as the absolute difference of EDGAR-Vulcan emissions for each region. Figure 8 shows the difference between “incorrect” prior (EDGAR)

uncertainties assumed for both ffCO₂ and bioCO₂ in all regions, using both flask and OCO-2 observations in the inversion. Here significant reductions in fractional uncertainty (from 100% in the prior for each region to between 5 and 50% in the posterior) were obtained for ffCO₂ in several regions (i.e., 3, 6, 7, 11, 12, 14, and 16) in May, with somewhat smaller reductions in November. This had the effect of reducing uncertainties in statewide California total ffCO₂ emissions from prior uncertainties of 41% and 40% (estimated from quadrature sum of 100% regional uncertainties) to the posterior uncertainties of 6.7% and 7.2% in May and November, respectively. For bioCO₂, significant reductions in posterior uncertainty (from 100% in prior to between 5% and 50% in posterior) were obtained

Table 6. Posterior Estimates of Bias in State Total Estimates of Fossil Fuel CO₂ Emissions (Tg C yr⁻¹) Obtained for Inversion Experiments by Using Vulcan Emissions to Simulate (True) Observations and Prior Predicted Signals Calculated With Either EDGAR or Flat Flux (1 Mmol m⁻² s⁻¹) Emission Maps^a

	Prior-True Exchange	Prior Uncertainty	Posterior-True Exchange	Posterior Uncertainty
<i>May</i>				
EDGAR prior	8.6	11.7	-3.1	4.6
Flat flux prior	73.4	42.5	28.9	20.9
<i>November</i>				
EDGAR prior	8.2	12.5	-4.7	4.7
Flat flux prior	73	42	4.4	16.4

^aIn each case, prior model uncertainty for the 16 regions inside California is calculated as the difference between the incorrect prior and true (Vulcan) emissions for that region.

and “true” (Vulcan) emissions and the difference of posterior minus Vulcan emissions for November 2010 after inversion. The posterior emissions are significantly improved from the prior emissions in regions 7, 12, 14, and 16, though slightly worse in region 10. As shown in Table 6, the resulting reductions in bias and uncertainty for state total ffCO₂ emissions range from “incorrect” prior minus “true” biases of 8.6 ± 11.7 and 8.2 ± 12.5 Tg C yr⁻¹ to posterior minus “true” errors of -3.1 ± 4.6 and -4.7 ± 4.7 Tg C yr⁻¹ in May and November, respectively. Here we

note that the EDGAR-Vulcan differences are computed by using monthly specific values for emissions from the Vulcan 2.2 data set that differ from the annual mean emissions shown in Table 2. We then repeated the prior model bias test, here computing the “incorrect” prior model signals by using a spatially uniform ffCO₂ flux = 1 μmol m⁻² s⁻¹ for all areas of California. As before, we estimated prior uncertainties on prior emissions as the difference from “true” Vulcan emissions. In this case, the inversion adjusted posterior emissions were larger but consistent with “true” emissions, with “prior” minus “true” emissions of 73 ± 43 Tg C yr⁻¹ and posterior minus “true” error of 29 ± 21 and 4.4 ± 16.4 Tg C yr⁻¹ for total California ffCO₂ emissions in May and November, respectively. In both of the above cases, the inversions using incorrect priors produce posterior emissions that are substantially closer to the true emissions, but only if the prior uncertainties are set large enough to encompass biases in the prior model.

Second, we tested the effect of some hypothetical CO₂ observation biases due to measurement error or inaccurate background subtraction with results shown in Table 7. In case (a) we applied a 1.1 multiplicative gain error to flask and OCO-2 observations together, mimicking a systematic underestimation in the strength of the footprints (e.g., due to systematic uncertainties in boundary layer depth and/or average wind speed). Here the estimated posterior estimates of CO₂ exchange were increased by ~10% in regions where the observations provide constraints on ffCO₂ emissions in regions 7, 12, 14, and 16 (not shown). The resulting posterior biases in statewide ffCO₂ emissions were 6.0 ± 4.0 and 6.0 ± 4.6 Tg C yr⁻¹ and biases in bioCO₂ were -9.6 ± 5.6 and 9.5 ± 8.5 Tg C yr⁻¹ in May and November, respectively. In case (b) we added a systematic +0.5 ppm bias to the flask observations and conducted a flask only inversion, mimicking a systematic error in flask measurement background subtraction. Here the California total posterior ffCO₂ emissions increased by 6.7 ± 4.1 and 4.1 ± 4.6 Tg C yr⁻¹ in May and November, respectively. Here posterior biosphere exchange

Table 7. Posterior-Prior Estimates of Bias in State Total Estimates of Fossil Fuel and Biosphere CO₂ Exchanges (Tg C yr⁻¹) Obtained for Inversion With Both Flask and OCO-2 Observations Scaled by a Factor of 1.1, Inversion Using Only Flask Observations Biased by +0.5 ppm, and Inversion Using Only OCO-2 Observations Biased by +0.5 ppm

	Fossil Fuel		Biosphere	
	Posterior-True Exchange	Posterior Uncertainty	Posterior-True Exchange	Posterior Uncertainty
<i>May</i>				
x1.1 footprint strength	6.04	4.06	-9.62	5.58
Flask + 0.5 ppm	6.67	4.11	0.23	5.77
OCO2 + 0.5 ppm	2.12	6.82	49.04	23.08
<i>November</i>				
x1.1 footprint strength	6.01	4.57	9.51	8.52
Flask + 0.5 ppm	4.14	4.62	3.71	8.75
OCO2 + 0.5 ppm	1.22	7.13	4.93	20.47

increased slightly by 0.23 ± 5.8 and $3.7 \pm 8.8 \text{ Tg C yr}^{-1}$ in May and November. In case (c) we added a systematic 0.5 ppm bias to the OCO-2 observations alone, mimicking an incorrect observational bias correction. Here statewide California total posterior ffCO_2 was biased 2.1 ± 6.8 and $1.2 \pm 7.1 \text{ Tg C yr}^{-1}$ in May or November, and biosphere exchange was biased 49 ± 23.1 and $4.9 \pm 20.5 \text{ Tg C yr}^{-1}$ in May and November, respectively. Although not shown in the table, we note that adding unbiased flask observations to the test with biased OCO-2 observations reduced the posterior biases in bioCO_2 to $<1 \text{ Tg C yr}^{-1}$.

4. Discussion

These simulation experiments suggest that the combination of $^{14}\text{CO}_2$ and total CO_2 measurements from a network of towers and XCO_2 measurements from OCO-2 can be effective in improving upon prior flux estimates for both fossil fuel emissions and net biosphere CO_2 exchange in California. Here the towers provide good coverage of major urban regions of California but comparatively sparse coverage of rural regions, while OCO-2 provides somewhat more rural coverage. In particular, the posterior uncertainties obtained from this analysis suggest that the prototype atmospheric inversion system could reduce the posterior uncertainties in California total CO_2 exchange to $\sim 5\text{--}14\%$ on the monthly average time scale with an ability to differentiate true fluxes from incorrect prior fluxes for major emitting regions using the observation and inversion system, provided that prior uncertainties are not underestimated. We also found that the posterior flux uncertainties were only moderately sensitive to increases in the prior uncertainty and to increases in the model-measurement uncertainty but that hypothetical biases in bioCO_2 and ffCO_2 signals created corresponding errors in posterior CO_2 exchanges. These last points suggest that inversions using specified prior uncertainties should include a sensitivity test varying prior uncertainties or use of a hierarchical Bayesian inversion method that allows dynamic adjustment of prior uncertainties [Jeong *et al.*, 2016].

The posterior uncertainty in ffCO_2 emissions of 5–6% on monthly time scales suggests that the inversion system could be effective in evaluating fossil fuel emission data products and emission reduction policies such as AB-32 in California, if observations are sustained and systematic errors can be controlled so that uncertainties are reduced over time. For example, the AB-32 emission reduction target is approximately 6% of total greenhouse gas emissions from 2013 to 2020, while future plans involve much larger emission reductions for 2030 (40% from 2020 to 2030) and 2050 (80% from 2020 to 2050). In addition, sustained observations will be needed to capture seasonal variations in fossil and biosphere CO_2 exchanges. Although not addressed in this analysis, targeted satellite observations of XCO_2 in large urban environments have the potential to reduce posterior emission uncertainties [e.g., Kort *et al.*, 2013], though careful attention to bias corrections and uncertainties will be required.

For bioCO_2 , the atmospheric inversion system produced posterior uncertainties of 6% to 12% of prior values, depending on season, suggesting that deployment of the system would improve estimates of the net bioCO_2 exchange from diverse ecosystems in California, particularly with year-round, sustained measurements. We note that OCO-2 provides coverage for some regions that are not effectively sampled by towers, likely allowing detection of spatial patterns due to management or climate change mitigation strategies that are not accurately captured in models for biosphere CO_2 exchange. In this respect, future missions such as OCO-3 on the International Space Station, and a recently selected geostationary satellite over the Americas (GeoCARB), offer the potential to improve spatial coverage of the California and the continental U.S. [Polonsky *et al.*, 2014].

As emphasized above, systematic uncertainties will need to be carefully controlled to achieve emission estimates with accuracy of 5% or better. For example, Basu *et al.* [2016] found that random error in estimates of U.S. continental annual ffCO_2 emissions could be reduced to below 5% by using roughly 400 radiocarbon samples per month at sites spread across the continental US, such that many areas are more sparsely covered than in this study. However, the authors found that the systematic difference in emission estimates derived from two different transport models was greater than 10%. While speculative, some aspects of systematic bias might be sufficiently similar from year to year that interannual emission trends might be detected. However, quantifying the sign, magnitude, and stability of systematic biases in regional transport models at the level of a few percent will be a significant challenge.

Acknowledgments

We gratefully acknowledge Jim Collatz and Andrew Jacobson for producing the CASA and Carbon Tracker biosphere CO₂ exchanges used in this work and for insightful comments on the manuscript. We also thank John Lin, Christoph Gerbig, Steve Wofsy, Janusz Eluszkiewicz, and Thomas Nehrkorn for making the STILT code publicly available; Krishna Muriki for assistance running the WRF-STILT models on the LBNL-Lawrencium cluster; and two anonymous reviewers for valuable suggestions that improved the paper. All prior CO₂ emission models used in this simulation study are available on websites listed in the references. Simulated CO₂ signals calculated with Vulcan and CASA biosphere CO₂ fluxes for OCO-2 and tower receptors are being made available at the Oak Ridge DAC (<https://doi.org/10.3334/ORNLDAAC/1381>). This study was supported by the NASA CMS program (NNH13ZDA001N) under U.S. Department of Energy contract DE-AC02-05CH11231.

References

- Andres, R. J., T. A. Boden, and D. Higdon (2014), A new evaluation of the uncertainty associated with CDIA estimates of fossil fuel carbon dioxide emission, *Tellus B*, 66, 23,616, doi:10.3402/tellusb.v66.23616.
- Asefi-Najafabady, S., P. J. Rayner, K. R. Gurney, A. McRobert, Y. Song, K. Coltin, J. Huang, C. Elvidge, and K. Baugh (2014), A multiyear, global gridded fossil fuel CO₂ emissions data product: Evaluation and analysis of results, *J. Geophys. Res. Atmos.*, 119, 10,213–10,231, doi:10.1002/2013JD021296.
- Basu, S., J. B. Miller, and S. Lehman (2016), Separation of biospheric and fossil fuel fluxes of CO₂ by atmospheric inversion of CO₂ and ¹⁴CO₂ measurements: Observation system simulations, *Atmos. Chem. Phys.*, 16(9), 5665–5683, doi:10.5194/acp-16-5665-2016.
- Boden, T. A., G. Marland, and R. J. Andres (2016), *Global, Regional, and National Fossil-Fuel CO₂ Emissions*, Carbon Dioxide Information Analysis Center, Oak Ridge Natl. Lab., U.S. Dep. of Energy, Oak Ridge, Tenn., doi:10.3334/CDIAC/00001_V2016.
- Brioude, J., et al. (2013), Top-down estimate of surface flux in the Los Angeles Basin using a mesoscale inverse modeling technique: Assessing anthropogenic emissions of CO, NO_x and CO₂ and their impacts, *Atmos. Chem. Phys.*, 13(7), 3661–3677.
- California Air Resources Board (CARB) (2015), California Air Resources Board: Emissions inventory data. [Available at <http://www.arb.ca.gov/cc/inventory/data/data.htm>.]
- Collatz, J., et al. (2013), CASA GFED3 MERRA fluxes. [Available at <http://nacp-files.nacarbon.org/nacp-kawa-01/>]
- Crisp, D., et al. (2017), The on-orbit performance of the Orbiting Carbon Observatory-2 (OCO-2) instrument and its radiometrically calibrated products, *Atmos. Meas. Tech.*, 10, 59–81, doi:10.5194/amt-10-59-2017.
- Emission Database for Global Atmospheric Research (EDGAR) (2011), EDGAR Greenhouse Gas Emissions Inventory v4.2. [Available at <http://edgar.jrc.ec.europa.eu/index.php>.]
- Frankenberg, C., et al. (2015), The Orbiting Carbon Observatory (OCO-2): Spectrometer performance evaluation using pre-launch direct sun measurements, *Atmos. Meas. Tech.*, 8, 301–313.
- Göckede, M., D. P. Turner, A. M. Michalak, D. Vickers, and B. E. Law (2010), Sensitivity of a subregional scale atmospheric inverse CO₂ modeling framework to boundary conditions, *J. Geophys. Res.*, 115, D24112, doi:10.1029/2010JD014443.
- Graven, H. D., T. P. Guilderson, and R. F. Keeling (2007), Methods for high-precision ¹⁴C AMS measurement of atmospheric CO₂ at LLNL, *Radiocarbon*, 49(2), 349–356.
- Graven, H. D., T. P. Guilderson, and R. F. Keeling (2012), Observations of radiocarbon in CO₂ at seven global sampling sites in the Scripps flask network: Analysis of spatial gradients and seasonal cycles, *J. Geophys. Res.*, 117, D02303, doi:10.1029/2011JD016535.
- Gurney, K. R., D. L. Mendoza, Y. Zhou, M. L. Fischer, C. C. Miller, S. Geethakumar, and S. de la Rue du Can (2009), High resolution fossil fuel combustion CO₂ emission fluxes for the United States, *Environ. Sci. Technol.*, 43(14), 5535–5541.
- Hogue, S., E. Marland, R. J. Andres, G. Marland, and D. Woodard (2016), Uncertainty in gridded CO₂ emissions estimates, *Earth's Future*, doi:10.1002/2015EF000343, in press.
- Hsueh, D. Y., N. Y. Krakauer, J. T. Randerson, X. Xu, S. E. Trumbore, and J. R. Southon (2007), Regional patterns of radiocarbon and fossil fuel-derived CO₂ in surface air across North America, *Geophys. Res. Lett.*, 34, L02816, doi:10.1029/2006GL027032.
- Jeong, S., Y.-K. Hsu, A. E. Andrews, L. Bianco, P. Vaca, J. M. Wilczak, and M. L. Fischer (2013), A multitower measurement network estimate of California's methane emissions, *J. Geophys. Res. Atmos.*, 118, 11,339–11,351, doi:10.1002/jgrd.50854.
- Jeong, S., et al. (2016), Estimating methane emissions in California's urban and rural regions using multitower observations, *J. Geophys. Res. Atmos.*, 121, 13,031–13,049, doi:10.1002/2016JD025404.
- Keeling, C. D., S. C. Piper, R. B. Bacastow, M. Wahlen, T. P. Whorf, M. Heimann, and H. A. Meijer (2001), *Exchanges of Atmospheric CO₂ and ¹³CO₂ With the Terrestrial Biosphere and Oceans From 1978 to 2000. I. Global Aspects*, Springer, New York.
- Konovalov, I. B., E. V. Berezin, P. Ciaia, G. Broquet, R. V. Zhuravlev, and G. Janssens-Maenhout (2016), Estimation of fossil-fuel CO₂ emissions using satellite measurements of "proxy" species, *Atmos. Chem. Phys.*, 16, 13,509–13,540.
- Kort, E. A., W. M. Angevine, R. Duren, and C. E. Miller (2013), Surface observations for monitoring urban fossil fuel CO₂ emissions: Minimum site location requirements for the Los Angeles megacity, *J. Geophys. Res. Atmos.*, 118, 1577–1584, doi:10.1002/jgrd.50135.
- LaFranchi, B. W., et al. (2013), Constraints on emissions of carbon monoxide, methane, and a suite of hydrocarbons in the Colorado Front Range using observations of ¹⁴CO₂, *Atmos. Chem. Phys.*, 13, 11,101–11,120.
- Le Quééré, C., et al. (2015), Global Carbon Budget 2015, *Earth Syst. Sci. Data*, 7(2), 349–396, doi:10.5194/essd-7-349-2015.
- Levin, I., B. Kromer, M. Schmidt, and H. Sartorius (2003), A novel approach for independent budgeting of fossil fuel CO₂ over Europe by ¹⁴CO₂ observations, *Geophys. Res. Lett.*, 30(23), 2194, doi:10.1029/2003GL018477.
- Li, J., D. M. Cunnold, H.-J. Wang, R. F. Weiss, B. R. Miller, C. Harth, P. Salameh, and J. M. Harris (2005), Halocarbon emissions estimated from Advanced Global Atmospheric Gases Experiment measured pollution events at Trinidad Head, California, *J. Geophys. Res.*, 110(D14), doi:10.1029/2004JD005739.
- Lin, J. C., et al. (2003), A near-field tool for simulating the upstream influence of atmospheric observations: The Stochastic Time-Inverted Lagrangian Transport (STILT) model, *J. Geophys. Res.*, 108(D16), 4493, doi:10.1029/2002JD003161.
- Liu, J., et al. (2014), Carbon monitoring system flux estimation and attribution: Impact of ACOS-GOSAT XCO₂ sampling on the inference of terrestrial biospheric sources and sinks, *Tellus B*, 66, 22,486, doi:10.3402/tellusb.v66.22486.
- Nehrkorn, T., J. Eluszkiewicz, S. C. Wofsy, J. C. Lin, C. Gerbig, M. Longo, and S. Freitas (2010), Coupled weather research and forecasting – stochastic time-inverted lagrangian transport (WRF-STILT) model, *Meteorol. Atmos. Phys.*, 107(1), 51–64, doi:10.1007/s00703-010-0068-x.
- Newman, S., et al. (2013), Diurnal tracking of anthropogenic CO₂ emissions in the Los Angeles Basin megacity during spring 2010, *Atmos. Chem. Phys.*, 13(8), 4359–4372.
- O'Brien, D. M., I. Polonsky, C. O'Dell, and A. Carheden (2009), Orbiting Carbon Observatory (OCO), algorithm theoretical basis document: The OCO simulator, Technical Report, ISSN 0737-5352-85, Cooperative Institute for Research in the Atmosphere, Colorado State Univ. [Available at ftp://ftp.cira.colostate.edu/ftp/TTaylor/publications/20090813_OCO_simulator.pdf.]
- Oda, T., and S. Maksyutov (2011), A very high-resolution (1 km × 1 km) global fossil fuel CO₂ emission inventory derived using a point source database and satellite observations of nighttime lights, *Atmos. Chem. Phys.*, 11, 543–556, doi:10.5194/acp-11-543-2011.
- Pacala, S. W., et al. (2010), Verifying greenhouse gas emissions: Methods to support international climate agreements, Committee on Methods for Estimating Greenhouse Gas Emissions, National Research Council, National Academy of Sciences, Washington, D. C.
- Polonsky, I. N., D. M. O'Brien, J. B. Kumer, C. W. O'Dell, and the geoCARB Team (2014), Performance of a geostationary mission, geoCARB, to measure CO₂, CH₄ and CO column-averaged concentrations, *Atmos. Meas. Tech.*, 7, 959–981, doi:10.5194/amt-7-959-2014.
- Potter, C. (2010), The carbon budget of California, *Environ. Sci. Policy*, 13(5), 373–383.
- Taylor, T. E., et al. (2016), Orbiting Carbon Observatory-2 (OCO-2) cloud screening algorithms: Validation against collocated MODIS and CALIOP data, *Atmos. Meas. Tech.*, 9, 1–17, doi:10.5194/amt-9-1-2016.

- Turnbull, J. C., J. B. Miller, S. J. Lehman, P. P. Tans, R. J. Sparks, and J. Southon (2006), Comparison of $^{14}\text{CO}_2$, CO, and SF₆ as tracers for recently added fossil fuel CO₂ in the atmosphere and implications for biological CO₂ exchange, *Geophys. Res. Lett.*, *33*, L01817, doi:10.1029/2005GL024213.
- Turnbull, J. C., et al. (2011), Assessment of fossil fuel carbon dioxide and other anthropogenic trace gas emissions from airborne measurements over Sacramento, California in spring 2009, *Atmos. Chem. Phys.*, *11*, 705–721.
- van der Werf, G. R., J. T. Randerson, L. Giglio, G. J. Collatz, M. Mu, P. S. Kasibhatla, D. C. Morton, R. S. DeFries, Y. Jin, and T. T. van Leeuwen (2010), Global fire emissions and the contribution of deforestation, savanna, forest, agricultural, and peat fires (1997–2009), *Atmos. Chem. Phys.*, *10*, 11,707–11,735.
- Winker, D., et al. (2010), The CALIPSO mission: A global 3D view of Aerosols and Clouds, *Bull. Am. Meteorol. Soc.*, *91*, 1211–1229, doi:10.1175/2010BAMS3009.1.
- Wolf, J., T. O. West, Y. Le Page, G. P. Kyle, X. Zhang, G. J. Collatz, and M. L. Imhoff (2015), Biogenic carbon fluxes from global agricultural production and consumption, *Global Biogeochem. Cycles*, *29*, 1617–1639, doi:10.1002/2015GB005119.
- Wu, L., G. Broquet, P. Ciais, V. Bellassen, F. Vogel, F. Chevallier, I. Xueref-Remy, and Y. Wang (2016), What would dense atmospheric observation networks bring to the quantification of city CO₂ emissions?, *Atmos. Chem. Phys.*, *16*(12), 7743–7771, doi:10.5194/acp-16-7743-2016.